



16th International Conference on Greenhouse Gas Control Technologies, GHGT-16

23rd -27th October 2022, Lyon, France

Simulations on Industrial Scale CO₂ Capture Vacuum Pressure Swing Adsorption using MIL-160(AI)

Arnaud Henrotin^a, Nicolas Heymans^a, Shyamapada Nandi^b, Farid Nouar^b, Georges Mouchaham^b, Christian Serre^b, Guy De Weireld^a

^aService de Thermodynamique et Physique Mathématique, Faculté Polytechnique, Université de Mons, 7000 Mons, Belgique

^bInstitut des Matériaux Poreux de Paris, École Normale Supérieure, ESPCI Paris, CNRS, PSL University, 75005 Paris, France

Abstract

Nowadays, power generation and carbon-intensive industries (steel plants, cement plants, lime ...) are responsible for around 50% of anthropogenic CO₂ emissions to Earth's atmosphere that mainly contributes to global warming. So, the reduction of CO₂ emissions from industries is crucial. Absorption-regeneration amine-based process, the benchmark solution, suffers from high energy penalties that leads adsorption process a promising alternative thanks to improvement of process design and development of new materials. Among these materials, MOFs appears as very promising material for both gas separation and purification. In the present work, the performance of the MIL-160(AI) produce at large scale were evaluated by adsorption isotherm measurements and breakthrough curve experiment. A modelling procedure was applied to both experiments to determine the CO₂ and N₂ adsorption isotherm parameters and kinetic parameters on the adsorbent. The parameters obtained were used to simulate a VPSA process at an industrial scale (100 Nm³/h of flue gas, 15% of CO₂) to evaluate the process performance of MIL-160(AI). Two different configurations were simulated for this study: a 2-stage VPSA process with 2 columns using 5 steps, and a 1-stage VPSA process with 3 columns and 6 steps. These configurations have been investigated and optimized to reach the targets of such a process: CO₂ purity of 95% and recovery of 90% with the lowest energy consumption and highest productivity. After a first optimization of these processes based on a design of experiments, the targets are close for the 2-stage VPSA process and reached for the 3bed-6step cycle. This last cycle can be optimized to promote energy consumption (393.1 kJ/kgCO₂) or productivity (0.1877 kgCO₂/(kg_{ads}.h)). These results confirm the promising potential of this adsorbent for the use at an industrial scale.

Keywords: CO₂ capture; VPSA; MOF; Process optimisation; Parametric study; Pilot unit

Nomenclature

b_0	Affinity constant [bar ⁻¹]
c_i	Concentration of compound i in gas phase [mol.m ⁻³]
$C_{v,g}$	Volumetric heat capacity of the gas [J.kg ⁻¹ .K ⁻¹]
$C_{v,s}$	Volumetric heat capacity of the solid [J.kg ⁻¹ .K ⁻¹]
$D_{L,i}$	Axial dispersion coefficient for compound i [m ² .s ⁻¹]
d_p	Diameter of the adsorbent [m]
ϵ_b	Porosity of the adsorption bed []
η	Efficiency of compressor/vacuum pump []
γ	Ratio of heat capacity []

ΔH	Heat of adsorption [$\text{J}\cdot\text{mol}^{-1}$]
h	Overall heat transfer coefficient between solid and gas [$\text{W}\cdot\text{m}^{-2}\cdot\text{K}^{-1}$]
h_w	Heat transfer coefficient between gas and wall [$\text{W}\cdot\text{m}^{-2}\cdot\text{K}^{-1}$]
$k_{LDF,i}$	Mass transfer coefficient of the compound i [s^{-1}]
λ_g	Thermal conductivity of the gas [$\text{W}\cdot\text{m}^{-1}\cdot\text{K}^{-1}$]
λ_s	Thermal conductivity of the solid [$\text{W}\cdot\text{m}^{-1}\cdot\text{K}^{-1}$]
P	Power [W]
Pr	Prandlt Number ($=\mu_g C_{p,g}/\lambda_g$)
p	Pressure [bar]
Q	Flowrate [$\text{mol}\cdot\text{s}^{-1}$]
\bar{q}_i	Average amount adsorbed of compound i in the pellet [$\text{mmol}\cdot\text{g}^{-1}$]
\bar{q}_i^*	Average amount adsorbed of compound i in the pellet at equilibrium [$\text{mmol}\cdot\text{g}^{-1}$]
q_{\max}	Maximum adsorbed amount [$\text{mmol}\cdot\text{g}^{-1}$]
Re	Reynolds Number ($=\rho_g v_0 d_p/\mu_g$)
μ_g	Dynamic viscosity of the gas [$\text{Pa}\cdot\text{s}$]
R	Perfect gas constant [$\text{J}\cdot\text{mol}^{-1}\cdot\text{K}^{-1}$]
ρ_g	Density of the gas [$\text{kg}\cdot\text{m}^{-3}$]
T	Temperature [K]
T_g	Temperature of the gas phase [K]
T_s	Temperature of the solid phase [K]
T_w	Temperature of the walls [K]
t	Time [s]
v	Interstitial velocity [m/s]
v_0	Superficial velocity [m/s]
z	Axial distance in the adsorption bed [m]

1. Introduction

Since the Industrial Revolution, human activities have led to a rapid change of the climate, mainly due to the release of greenhouse gas in the atmosphere. Among these gases, CO_2 is the main contributor to global warming, and the emissions of this gas should be reduced to limit global warming to 1.5°C above pre-industrial levels, as stated in the Paris Agreement. This objective can be achieved by a reduction of 50% of the anthropogenic CO_2 emissions (20 GtCO_2/yr) in 2035 and the net zero emission in 2055 followed by negative net emissions, according to the scenarios of the IPCC [1][2]. In 2019, the global CO_2 emission was about $43.05 \pm 3.3 \text{ GtCO}_2$ with 85% from fossil emissions. Carbon dioxide emissions come from different sources in varying quantities and concentrations. Nowadays, power generation and carbon-intensive industries (steel plants, cement plants, lime plant, ...) are responsible for around 50% of CO_2 emissions [3][4].

Focusing on the industrial sector, several solutions can be used to reduce the CO_2 emissions: increasing the renewable energies share, fuel switching from solid or liquid to gas, process efficiency improvement ... Nevertheless, during this transition, an efficient solution to reduce the CO_2 emissions while using fossil fuels, is to capture the CO_2 before it is released into the atmosphere. Capture processes are particularly interesting for reducing emissions from certain sources that cannot work without fossil fuels, such as certain industrial sectors where the temperatures to be reached are very high ($> 1000^\circ\text{C}$) and for which electric heating is not possible. In addition, a part of the CO_2 emitted from several industrial processes is unavoidable (such as decarbonation phase in cement plant or lime plant) even if the energy required comes from a renewable source. According to International Energy Agency projections, 17% of the carbon dioxide emissions reduction should be done by Carbon Capture and Storage (CCS) by 2035 [2][5][6][7].

Different processes for capturing the CO_2 from industrial sources can be found in the literature such as the pre-combustion or the oxy-combustion capture. Capture by post-combustion is currently the configuration which is the most widely studied and considered. In this configuration the CO_2 is captured at the end of a process before the flue gases are released into the atmosphere. This process is the most easily implemented on an existing installation

compared to the two other processes [7][8][9]. Among the gas separation techniques, the most well-established and understood technology is the post-combustion chemical absorption in solvents which are generally aqueous alkanolamine such as monoethanolamine (MEA) and N-methyldiethanolamine (MDEA). Carbon dioxide capture in amines can achieve a recovery rate of 90% with the purity of the CO₂ stream equal to 95-98%. Carbon capture by chemical absorption is already applied at commercial level, but the energy consumption of these units is not really communicated. At a lower scale, the best pilot plants use around 2.3-2.4MJ/kgCO₂ (URCASOL™ solvent) [7][10][11][12]. Several drawbacks are associated to the chemical absorption with amines. The solvents are generally unstable at high temperature leading to the decomposition of the amines and a decrease in performance over time. Moreover, amine solutions are corrosive and sensitive to contaminants such as SO₂, NO_x or O₂. Amine loss by aerosols and degradation products are also problematic in these processes due to their environmental hazards and toxicity. Nevertheless, the high energy consumption required for the solvent regeneration remains the main reason for the search of alternative capture technology [7][10][13]. In addition some industries that are not Seveso sites do not wish to become Seveso sites (Directive 96/82/EC) for the use and storage of amines.

Among the other technologies, adsorption processes are a promising alternative to amines solvents, allowing to decrease the energy penalty, cost, and environmental impact. Adsorption is already used in applications such as petrochemical, air separation or hydrogen purification and can be used for the separation of CO₂ in post-combustion [7][14][15]. Performance of adsorption processes is directly related to the material used. For post-combustion process, zeolites which are porous aluminosilicate materials show good CO₂ capacity and selectivity at low pressure and temperature making them suitable for capture processes. Nevertheless, zeolites are sensible to water due to their hydrophilic nature, reducing their capacity and active surface area [10][16].

A promising class of adsorbent material is the Metal Organic Frameworks (MOFs) due to their high surface areas and void volume, high porosity, finely tunable pore surface properties and industrial scalability. MOFs consist in a central metal atom (or cluster of atoms containing a metal) where organic ligands are linked by coordinate bonds to form a one, two or three-dimensional network. The large number of MOFs that can be synthesized has led to numerous research in the context of CO₂ capture to find materials which exhibit a high selectivity for CO₂, high CO₂ capacity, minimal energy penalties for regeneration, and a good chemical and mechanical stability [8][10]. The choice of the regeneration method is made based on economic and technical considerations. Thermal swing adsorption (TSA) allows the use of a cheap steam source or waste heat making this method attractive. However, TSA processes suffer from the long time needed to heating and cooling the bed, making it impossible for fast cycle. Therefore, the amount of adsorbent needed for a TSA process (and thus the investment costs) is higher than in pressure swing adsorption processes (PSA) which are more suitable for rapid cycling. The main drawback of PSA process is the mechanical energy required for modifying the pressure, being more expensive than the thermal energy. As a rule of thumb, PSA process is preferred when the most adsorbed compound as a concentration higher than a few per cent in the feed gas. An alternative configuration to the PSA process is the vacuum pressure swing adsorption (VPSA) process by regenerating the adsorbent under vacuum. This configuration allows to reduce the energy consumption of the process compared to a classical PSA [16][17].

In this context, the H2020-MOF4AIR project (<https://www.mof4air.eu/>) aims to develop and promote the use of MOFs for CO₂ capture in energy and industrial sectors. The project started in July 2019 and was initially planned to last 4 years. 14 partners are involved in the project, to develop the process of CO₂ capture with MOFs from the material synthesis to an industrial pilot scale. Several MOFs have been studied to be used in a VPSA process. MIL-160(Al) [18][19] have been selected after several experimental measurements at small scale proving its capacity to keep CO₂ capture properties in real conditions (presence of impurities as water, NO_x, SO₂).

In this work, the performance of MIL-160(Al) produces at large scale have been evaluated by CO₂ and N₂ pure component adsorption isotherms and breakthrough curve measurements with CO₂/N₂ (15/85) mixture. All the measurements carried out on the material (adsorption isotherms, breakthrough curves) were used to validate the model used for the simulation of the industrial unit. A complete simulation of VPSA process using the Linear Driving Force (LDF) model and ideal adsorbed solution theory (IAST) was performed on Aspen Adsorption® software to evaluate the performances of a VPSA process with MIL-160(Al) on an industrial scale (100 Nm³/h of flue gas). The flue gas specification used in the simulation (15% CO₂, 85% N₂, dry) is representative of the flue gases (after dust removal unit, De-SO_x and De-NO_x unit, and dehumidifying) coming from a fluid catalytic cracking (FCC) system in Technology Centre Mongstad pilot plant which is a demonstration site of the MOF4AIR project. Several

configurations with different numbers of columns and beds can be used in a VPSA cycle. The simplest configuration is a two columns configuration using the Skarstrom cycle [20]. Nevertheless, two successive units are required to reach the targets of recovery and purity. To increase the performance and reach the targets with a single unit, the 3 columns processes can be used. Several configurations exist with three adsorption bed such as the 3bed-5step cycle [21] or 3bed-7step cycle [22]. The 3bed-6step cycle was selected for this study. This cycle has been reported to show promising results for CO₂ capture, allowing to potentially meet the targets of purity and recovery [23][24]. Therefore, in this work, the 2bed-5step configuration, and the 3bed-6step have been investigated and optimized to study the influence of some variables and reach the targets of such a process: CO₂ purity of 95% and recovery of 90% with the lowest energy consumption.

2. Materials and methods

2.1. Experimental measurements

2.1.1. Materials

The material studied in this work is the MIL-160(Al) (Formula: Al(OH)(O₂C-C₄H₂O-CO₂) which is composed of an inorganic aluminum chain linked via five-membered ring 2,5 furan di-carboxylate ligand, forming helical chains, and pore size between 4 and 6 Å. This MOF has interacting sites for CO₂ (or H₂O) molecules which provides a good selectivity of CO₂ over N₂. This material is stable under water condition and has also been reported to be resistant to SO₂ where adsorption occurs for this compound with a higher selectivity than CO₂. The stability against H₂S is not fully known but molecular simulations tend to show that this adsorbent is not stable against this compound requiring pretreatments [18][19][25][26].

The MIL-160(Al) was provided by IMAP (Institut des Matériaux Poreux de Paris) and is shaped with 3% of polyvinyl butyral (PVB) as binder by wet granulation following the method described by the reference [27]. The materials obtained have a spherical shape with diameters varying between 1.4 and 2.5 mm. The BET surface of this shaped MOF is equal to 1130-1140 m²/g.

2.1.2. Gases

Carbon dioxide, nitrogen and helium were provided by Air Liquide Belgium with a purity of 99.999%.

2.1.3. Adsorption isotherms

Adsorption isotherm measurements for CO₂ and N₂ were performed by gravimetric techniques with a built in-house apparatus around a high-pressure magnetic suspension balance marketed by Rubotherm after in-situ outgassing overnight at 150° the column overnight at 150° under secondary vacuum. The system allows measurements of an adsorbent sample (around 1 g) in a pressure range of 0-150 bar and in a temperature range of 233.15-403.15 K. More details about the installation and the methodology can be found in literature [28].

Adsorption isotherms were measured at three temperatures (20°C, 30°C and 40°C) to consider the temperature dependency in the modelling. The CO₂ adsorption isotherms were measured between 0.01 and 1 bar, and N₂ adsorption isotherms between 0.1 and 50 bar. This wide range of pressure allows to use the IAST were the computation of the adsorbed amount at lower pressure than the actual pressure for the most adsorbed compound, and at higher pressure for the less adsorbed is necessary [29][30].

2.1.4. Breakthrough curves

The experimental set-up for CO₂/N₂ breakthrough curve measurements is represented in Figure 1. It is composed of a metallic column (height: 50 cm; diameter: 2.17 cm; volume: 180cm³) containing the adsorbent surrounded by a jacket in order to set the column temperature to a set point value, with a water bath. The gas mixture is generated using 2 mass flow controllers [D1 and D2] (Brooks Instrument: CO₂: 0-1 NL/min and N₂: 0-10 NL/min) and analyzed continuously by a mass spectrometer [MS] (InProcess Instruments – GAM 200 with a mass range from 1 to 200 amu). The mass spectrometer is calibrated before each set of measurements. A back-pressure controller [BP] (Brooks

Instrument) allows to set the pressure and to keep it constant in the column and a vacuum pump is used to regenerate the adsorbent under vacuum. There are 3 thermocouples inside the column (at 2, 22 and 42 cm from the inlet) to record the temperature.

The experimental method is as follows: The adsorbent is placed in the column and regenerated under vacuum by heating the column overnight at 150°C. The column is then pressurized with nitrogen until equilibrium is reached (constant temperature in the column). After pressurization, the CO₂/N₂ mixture is generated and analyzed with the mass spectrometer before the adsorption measurement. The mixture is then sent to the column to perform the breakthrough curve measurement. During the experiment, the pressure, temperatures, flow rates and CO₂ concentration are recorded.

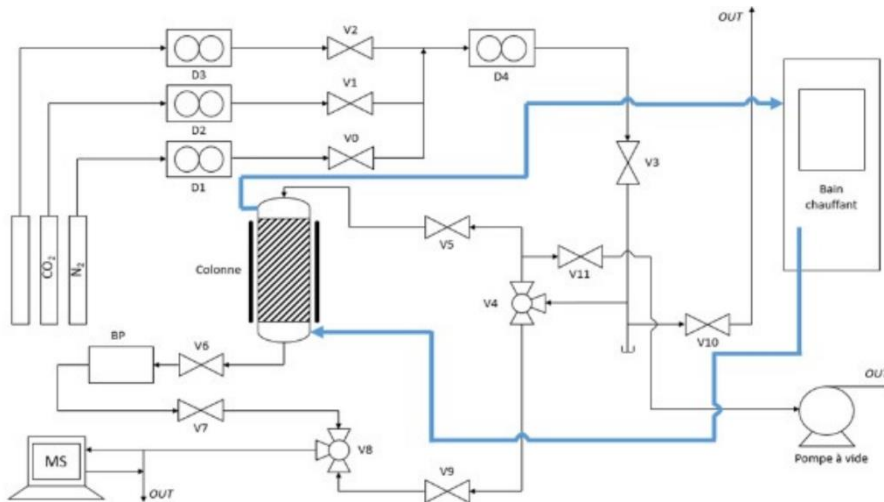


Fig. 1. Experimental set-up for CO₂/N₂ breakthrough curve measurements.

2.1.5. Vacuum pressure swing adsorption processes

2.1.5.1. Indicators and targets

Several indicators exist to evaluate the performance of an adsorption cycle. Four main indicators are:

- Recovery: Quantity of CO₂ retrieved in the product stream divided by the quantity of CO₂ in the feed stream for one cycle.
- Purity: Average composition in CO₂ of the product stream for one cycle.
- Productivity: Amount of CO₂ captured by grams of adsorbents used in the process and by hours.
- Energy consumption: Energy needed to capture one gram of CO₂. This indicator is more complex since it depends on the performance of the compressor and/or vacuum pump used. Moreover, there are different models which can be used to determine the energy consumption of a pump. The simplest model is an adiabatic and reversible compression. The compression power needed in this case is given by equation 1. By dividing the power required by the amount of CO₂ retrieved during one cycle, we obtain the energy consumption for the capture of one kilogram.

$$P_{comp} = \frac{1}{\eta} \frac{\gamma}{\gamma-1} RT \left[\left(\frac{p_{high}}{p_{low}} \right)^{\frac{\gamma-1}{\gamma}} - 1 \right] \cdot Q \quad (1)$$

The expected performances of a CO₂ capture unit are a recovery of 90% and a purity of 95% to compete with amine solvents. The energy consumption should be as low as possible to reduce the operating cost while the productivity should be as high as possible to reduce the investment cost [31].

2.1.5.2. 2-bed 5-step

The carbon capture with a two-bed configuration is based on a Skarstrom cycle [20] with an additional pressure equalization step for increasing the efficiency of the process and reduce the energy consumption [17]. In this configuration, two successive units are required to approach the targets of a CO₂ capture process [32][33]. The five steps of the cycle are as follows and represented in Figure 2:

- Adsorption: The flue gas is sent to the adsorption bed. The CO₂ is retained (adsorbed to the solid surface) and the stream at the outlet of the bed contains almost no CO₂. During the adsorption step, the amount of CO₂ adsorbed increases, and the concentration of CO₂ at the outlet can increase when the bed begins to breakthrough.
- Equalization: To reduce the energy consumption of the compressor or vacuum pump, a step of pressure equalization is made between the adsorption and blowdown. The bed in adsorption and the second bed in blowdown are connected to equalize the pressure and then reduce the work of compression and vacuum.
- Blowdown: The bed filled with CO₂ adsorbed is regenerated with a decrease of pressure during the blowdown step. The top of the bed is closed, and a vacuum pump connected to the bottom decreases the pressure and collect the CO₂ which is desorbed at low pressure.
- Purge: This step is intended to flush the gas (rich in CO₂) at the end of the blowdown with the gas leaving the adsorption bed (rich in N₂) to increase the recovery of carbon dioxide.
- Pressurization: After the blowdown step at low pressure and before the adsorption step at high pressure, a pressurization step is needed to increase the pressure inside the bed. This step should be as fast as possible.

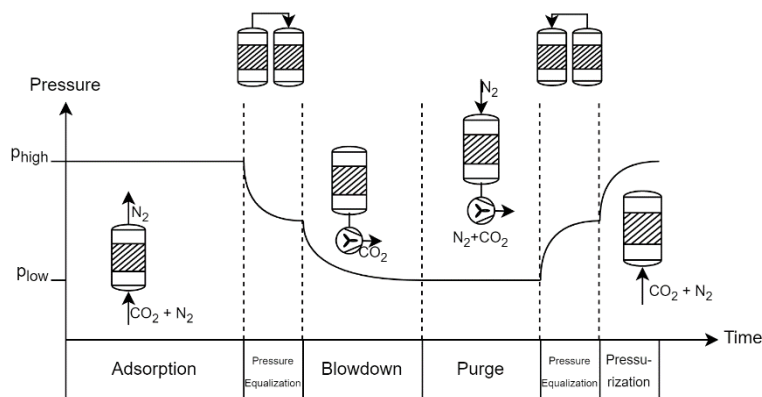


Fig. 2. Pressure levels and representation of each step for the 2-bed 5-step process

The time of each step is not independent the sum of the time of pressurization and adsorption are equal to the sum of the time of blowdown and purge. Since the bed is not working during the pressurization and equalization steps, these last must be as fast as possible.

2.1.5.3. 3-bed 6-step

The three-bed VPSA cycle with 6-step [24] aims to reach the targets of a CO₂ capture process with only 3 columns and a low energy consumption. The pressure levels of a bed during the cycle are represented in Figure 3. A new step called “light blowdown” is used to decrease the bed pressure to an intermediate pressure, the stream recovered during this step is not collected and sent to the atmosphere. The purpose of this step is to remove the nitrogen from the column without desorbing the CO₂.

A special characteristic of this cycle is the synchronisation of the purge and rinse steps. As represented in Figure 3, a part of the nitrogen stream retrieved from the adsorption step is used for the purge of a second bed. The stream recovered from the purge is then directly used for the rinse of the third bed after recompression. The aim of the rinse step is to flush the nitrogen at the end of the adsorption step with a CO_2 -rich stream to increase the overall purity of the recovered CO_2 . The pressurization step is also slightly different, using nitrogen from one bed in adsorption to increase the pressure of a second bed instead of flue gas.

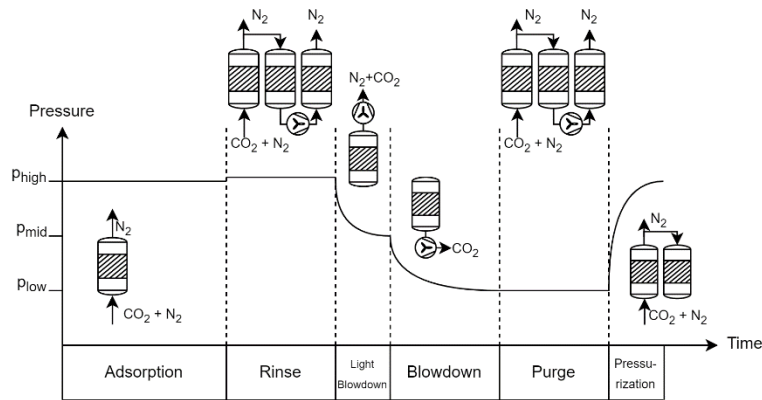


Fig. 3. Pressure levels and representation of each step for the 3-bed 6-step process

Step	Bed 1	Bed 2	Bed 3
1	Adsorption	Purge	Rinse
		Pressurization	Light Blowdown
			Blowdown
			Purge
2	Rinse	Adsorption	Purge
3	Light Blowdown		Pressurization
4	Blowdown		
5	Purge		
6	Pressurization	Light Blowdown	Adsorption
		Blowdown	

Fig. 4. State of the three beds during one cycle of 3-bed 6-step process.

From the Figure 4, a relationship between the steps can be made. The adsorption time is equal to the sum of the pressurization and purge times. Moreover, the purge and the rinse have the same duration since they are synchronous. The last relationship is the link between the pressurization time and the sum of the two blowdown steps.

2.2. Modelling

A modelling work was performed to determine equilibrium and kinetic parameters from adsorption isotherm measurements and breakthrough curve measurements, respectively. In second a second step, the parameters will be used for the modelling of a vacuum pressure swing adsorption process. This process modelling will allow to study the influence of different operating parameters, and to determine the optimum operating conditions for CO_2 capture.

2.2.1. Adsorption isotherms

Data obtained from adsorption isotherm measurements were modeled with a Langmuir model (equation 2) with a temperature dependency [34]. The parameters of the model were obtained with a fitting of the data with a nonlinear least-squares solver in Matlab©(lsqnonlin) using the trust region reflective algorithm. The algorithm searches the

minimum of the cost function describe by the sum of squared differences between measured adsorbed amount and modeled adsorbed amount with the parameters to be identified. In addition, a multistart procedure was used to perform the identification procedure with several initial conditions in order to avoid local minima. The 95% confidence intervals of parameters were determined by the Jacobian matrix provided by the solver. The results of the fitting were evaluated with the R-squared (equation 3) and the normalized root mean square deviation (NRMSD, equation 4) [35].

$$q = q_{\max} \frac{b_0 \exp\left(\frac{-\Delta H}{RT}\right)p}{1 + b_0 \exp\left(\frac{-\Delta H}{RT}\right)p} \quad (2)$$

$$R^2 = \frac{\sum_i^n (q_{exp,i} - q_{model,i})^2}{\sum_i^n (q_{exp,i} - q_{mean})^2} \quad (3)$$

$$NRMSD = \sqrt{\frac{\sum_i^n (q_{exp,i} - q_{model,i})^2}{n}} \quad (4)$$

2.2.2. Breakthrough curves

Breakthrough curves were modelled in Aspen Adsorption© V11 software to fit the experimental data and determine the kinetic parameters of adsorption. The adsorption bed is divided into 100 axial nodes for the resolution of the mass, momentum, and thermal balance across the bed. The assumptions for the modelling are:

- IAST is used for the co-adsorption prediction [28].
- The flow through the bed is represented by the axial dispersed plug flow model (equation 5) [36].
- The gas phase is represented with the Redlich-Kwong equation of state.[37]
- Ergun equation is used for the momentum balance (equation 6) [38].
- Linear driving force with a constant coefficient (no temperature dependency) is used for the mass transfer resistance (equation 7) [39].
- The column is non-isothermal with solid and gas conduction in the column and through the wall (equations 8 and 9). The external jacket is considered. The heat transfer coefficient between solid and gas is estimated by the Chilton-Colburn analogy [40] (equation 10), the external heat transfer coefficient is estimated with the Dittus-Boelter correlation [41][42] (equation 11) and the gas to wall heat transfer coefficient by Dixon model [43].

$$-D_{L,i} \frac{\partial^2 c_i}{\partial z^2} + \frac{\partial(v c_i)}{\partial z} + \frac{\partial c_i}{\partial t} + \left(\frac{1-\varepsilon_b}{\varepsilon_b}\right) \frac{\partial \bar{q}_i}{\partial t} = 0 \quad (5)$$

$$-\frac{dp}{dz} = \frac{150\mu_g(1-\varepsilon_b)^2}{\varepsilon_b^3 d_p^2} v_0 + \frac{1.75(1-\varepsilon_b)\rho_g}{\varepsilon_b^3 d_p} v_0^2 \quad (6)$$

$$\frac{\partial \bar{q}_i}{\partial t} = k_{LDF_i} (\bar{q}_i^* - \bar{q}_i) \quad (7)$$

$$-\frac{\lambda_g}{c_{v,g}} \frac{\partial^2 T_g}{\partial z^2} + v \frac{\partial T_g}{\partial z} + \frac{\partial T_g}{\partial t} + \left(\frac{1-\varepsilon_b}{\varepsilon_b}\right) \left(\frac{c_{v,s}}{c_{v,g}}\right) \frac{\partial T_s}{\partial t} = \left(\frac{1-\varepsilon_b}{\varepsilon_b}\right) \left(\frac{-\Delta H}{c_{v,g}}\right) \frac{\partial \bar{q}}{\partial t} - \frac{4h_w}{\varepsilon_b d_p c_{v,g}} (T_g - T_w) \quad (8)$$

$$c_{v,s} \frac{\partial T_s}{\partial t} = \frac{6h}{d_p} (T_g - T_s) + (-\Delta H) \frac{\partial \bar{q}}{\partial t} \quad (9)$$

$$Nu = 2 + 1.1 Pr^{1/3} Re^{0.6} \quad (10)$$

$$Nu = 0.023 Pr^{0.3} Re^{0.8} \quad (11)$$

The identification of the linear driving force coefficients for CO₂ and N₂ and thermal conductivity of the adsorbent was made by minimization of the sum of squared differences with the surrogate optimization algorithm (surrogateopt) in Matlab (between measured and modelled breakthrough curves). The concentration profile and the thermal profile obtained with the three temperature sensors of the adsorption bed were used for the identification procedure.

2.2.3. Vacuum pressure swing adsorption process

The two vacuum pressure swing adsorption cycles presented in Section 2.1.5 were modelled in Aspen Adsorption© V11 software with the same assumptions as the breakthrough curve modelling. The system studied is a CO₂ capture unit treating 100Nm³/h of a CO₂/N₂ mixture with 15% of CO₂ at 25°C. Several parameters were studied with a design of experiments to study their influence on the four indicators presented in Section 2.1.5.1 [44]. Each simulation was performed until the cyclic steady state was reached. Unlike the breakthrough curve, the simulated industrial column does not have a double jacket. Classical correlations of heat transfer in free convection were used [41][42].

For both cycles, the volume of the bed (20 to 120 L for the 2 columns cycle and 20 to 140 L for the 3 columns cycle), the length to diameter ratio (2 to 8), the adsorption pressure (1.1 to 2 bar) and the blowdown pressure (0.5 to 0.1 bar) were studied. For the 2bed-5step cycle, the adsorption time (30 to 200 s), purge time (10 to 190 s) and purge flow rate (20 to 80 Nm³/h) were studied in addition to the parameters above. For the 3bed-6step, the adsorption time (30 to 200 s), the purge time (10 to 190 s), the light blowdown time (10 to 190 s), the purge flow rate (20 to 80 Nm³/h), and the intermediate pressure (0.2 to 1.9 bar) were investigated.

3. Results and discussions

3.1. Adsorption isotherms

The adsorption isotherms obtained for CO₂ and N₂ at 20, 30 and 40°C are represented in Figure 5. The working capacity which is the difference between the partial pressure of CO₂ during adsorption and desorption can be computed from the experimental data. By taking an adsorption pressure of 1.1 bar and a blowdown pressure of 0.1 bar with a concentration of CO₂ of 15% at 30°C, the working capacity obtained is equal to 0.87 mmol/g of CO₂.

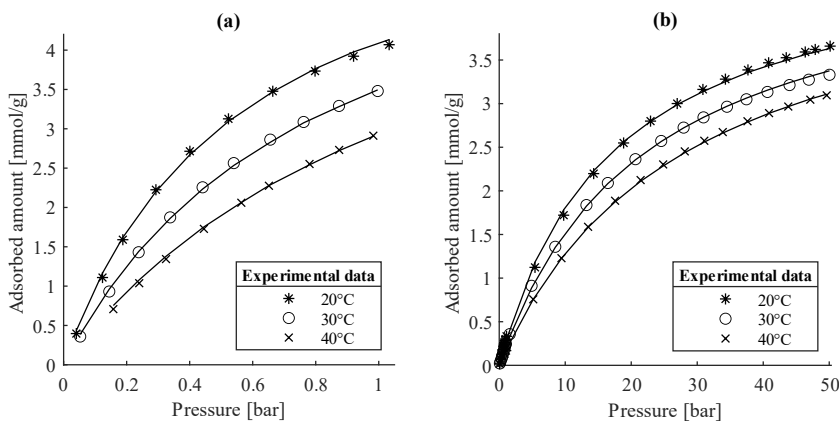


Fig. 5. Adsorption isotherms obtained for CO₂ (a) and N₂ (b) at three different temperatures (marks = experimental data, plain lines = modelling).

A Langmuir model with a temperature dependency was fitted to the experimental data with the procedure explained in the section 2.2.1. The parameters obtained in addition to the confidence intervals at 95% are given in the Table 1. The resulting model is also represented in Figure 5 by the solid lines. The model shows a good fitting, giving a value of R² equal to 99.88% for CO₂ and 99.95% for N₂. The values of NRMSD obtained are equal to 0.58% for CO₂ and equal to 0.35% for N₂.

Selectivity of the MIL-160(A1) can be computed with the Langmuir model by using the IAST Taking the operating conditions of the adsorption bed (1.1 bar, 30°C, 15% CO₂), the selectivity for CO₂ is equal to 36.7, showing a good affinity for CO₂ over nitrogen.

Table 1. Parameters obtained for Langmuir model with the experimental data.

Parameters	CO ₂	N ₂
q _{max} [mmol.g ⁻¹]	6.33 ± 0.15	4.85 ± 0.05
b ₀ [bar ⁻¹]	1.28e-5 ± 4.42e-6	1.89e-5 ± 4.49e-6
ΔH [J.mol ⁻¹ .K ⁻¹]	-28930 ± 930	-19640 ± 620

3.2. Breakthrough curve

Breakthrough curve was measured with the apparatus described in section 2.1.2 with 95.17g of adsorbent. The experiment was performed with a flow rate of 11.9 NL/h and a CO₂ molar fraction of 14.95%. The experimental results obtained are represented in Figure 6. In addition, the breakthrough curves obtained were shown to be reproducible.

The breakthrough curve was simulated as described in section 2.2.2 to determine the mass transfer coefficients in addition to the thermal conductivity of the adsorbent. The results of the fitting are shown in Figure 5 by the dashed line. In addition, the R² and NRMSD obtained for each curve are given in the Table 2. The fitting obtained has an excellent value for the breakthrough curve, and acceptable values for thermal profile, showing an overall good fitting of the experimental data. The parameters obtained from the fitting procedure are given in the Table 3.

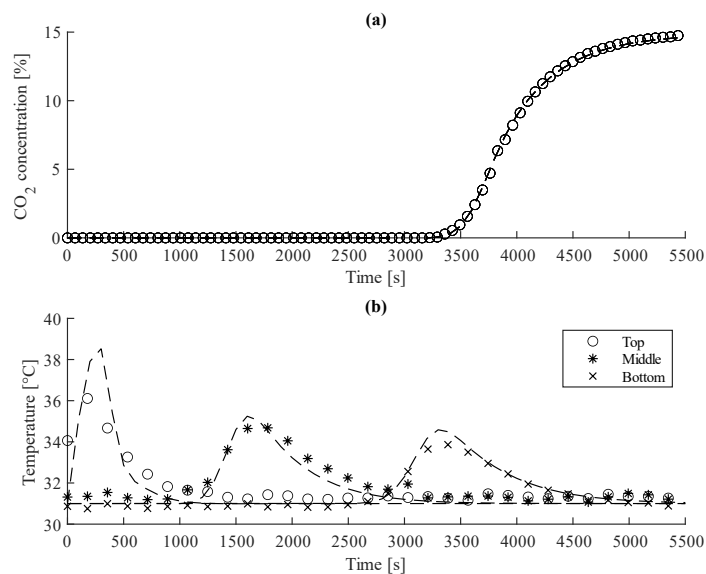


Fig. 6. Breakthrough curve (a) and thermal profile (b) obtained from breakthrough curve experiment and modelling (marks = experimental data, dashed lines = modelling results).

Table 2. R² and NRMSD obtained for breakthrough curve fitting

	R ²	NRMSD
Breakthrough curve	99.9%	1.55%
Top temperature	71.6%	4.06%
Middle temperature	88.8%	1.38%
Bottom temperature	95.7%	0.73%

Table 3. Parameter obtained from the fitting of breakthrough curves experiment

Parameters	Value
$k_{LDF} \text{ CO}_2$ [s^{-1}]	0.35
$k_{LDF} \text{ N}_2$ [s^{-1}]	0.03
λ [$\text{W}\cdot\text{m}^{-1}\cdot\text{K}^{-1}$]	0.13

3.3. Vacuum pressure swing adsorption process

3.3.1. 2-bed 5-step

The parameters listed in section 2.2.5 were studied by a design of experiments. 84 simulations were performed, and the results were fitted to a response surface. The response surface is in accordance with the results obtained from the simulation, showing a R^2 of 97% for purity and energy consumption, and 96% for recovery and productivity.

The Figure 7 shows two pareto plots obtained from the response surface for two levels of adsorption pressure (1.1 and 2 bar), and different volumes of the adsorption bed (20 to 120 L). For both plots, the increase of volume shows an increase of purity for a given recovery until 80 L. For the 1.1 bar plot, the 80 L and 100 L curves are merged showing that an increase in volume no longer increases the performance of the cycle. Moreover, the 120 L curve is below the 100 L curve, indicating a decrease in performance. This suggests that there is an optimum volume beyond which the maximum purity reachable decrease for a given recovery. For the 2 bar plot, the same behavior is observed with a merge of the 80,100 and 120 L curves. The 100 L curve is slightly above the 80 and 120 L curve for recovery lower than 90%. The increase of pressure seems to increase the purity for a given recovery. A difference of +- 5% of purity increase by increasing the pressure from 1.1 to 2 bar is observed. Nevertheless, this increase of pressure has a detrimental effect on the energy consumption of the VPSA cycle.

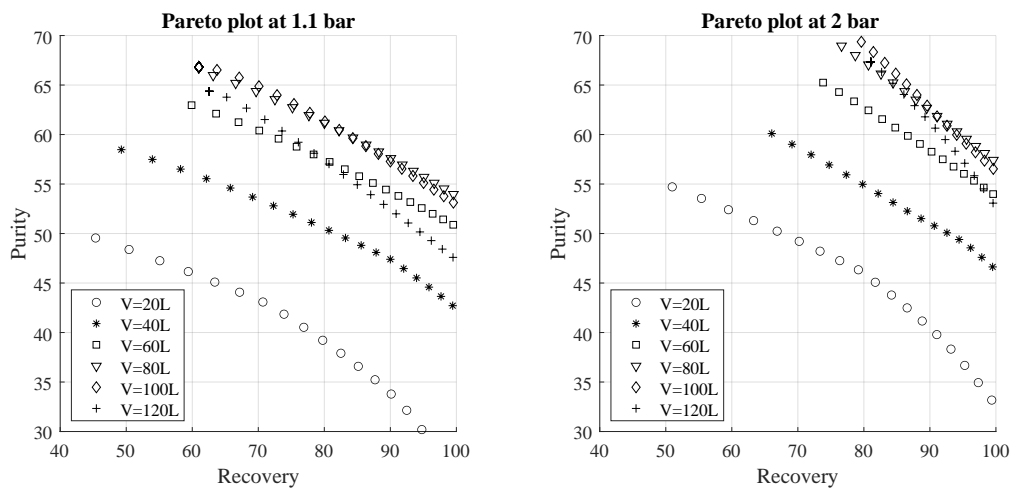


Fig. 7. Purity versus recovery obtained for different volumes of individual adsorption bed at two different adsorption pressure.

The results obtained doesn't allow to reach the desired performance of a CO₂ capture process. The 2bed-5step can reach high recovery, but the purity obtained at high recovery are significantly below the target of 95%. To reach this value, a second stage of a 2bed-5step VPSA was studied with the same methodology as the first unit. 106 additional simulations were performed and fitted to a response surface to study the second unit. The fittings obtained are good showing a R² of 95% for purity and recovery, 93% for productivity and 96% for energy consumption.

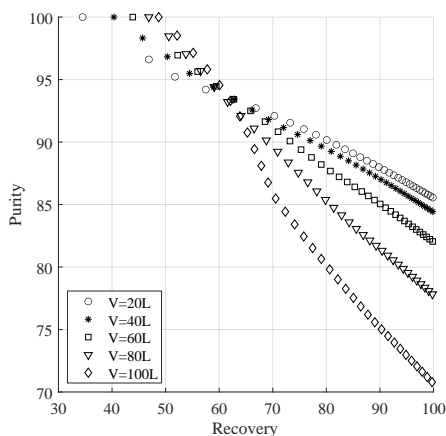


Fig. 8. Purity versus recovery obtained for different volumes of individual adsorption bed for the second unit of the 2bed-5step cycle.

Figure 8 gives the pareto plot of the recovery and purity obtained with different volumes of the second unit. This pareto plot was obtained by optimizing the parameters of the first unit for a fixed bed volume of 80 L, and the parameters of the second. The high pressure of the first and second unit can vary in this graph. The CO₂ concentration at the entrance of the second unit is equal to the purity obtained from the first unit, and the feed flowrate of the second unit is obtained from the recovery and the purity of the first unit.

As observed, for recovery higher than 90%, the decrease of the volume of the adsorption bed seems to increase the purity. This effect is particularly visible between 60 and 100 L and seems to decrease below 60 L. One possible explanation is that the heat generated by the adsorption is better dissipated in a smaller volume. Since the CO₂ concentration at the inlet of the second unit is between 40 and 60%, the heat released by the adsorption in the second unit is much more important, thus decreasing the adsorption capacity on columns that dissipate temperature poorly.

The best point obtained has a recovery of 90.1% for a purity of 87.9%, the productivity is equal to 0.1240 kgCO₂/(kg_{ads}.h) and the energy consumption to 988.7 kJ/kgCO₂. The targets are not totally met with this cycle, the energy consumption obtained is also very high making it difficult to compete with other capture processes. This cycle could nevertheless find applications where less purity is required such as the reuse of CO₂ (CCU) if the energy consumption is lowered.

3.3.2. 3-bed 6-step

The second cycle studied is the 3-bed 6-step. 302 simulations were performed, and the results were fitted to a response surface. The surface response is in accordance with the results obtained from the simulation, showing a R² of 92% for purity, 85% for recovery, 86% for productivity and 93% for energy consumption. From this surface response, a pareto plot was made for an adsorption pressure of 1.1 bar and 2 bar represented in Figure 9. As for the 2 columns cycle, the increase of bed volume seems to increase the purity obtained for a given recovery. At 1.1 bar, this effect is visible between 20 and 80 L, we can also observe that a recovery of at least 90% can only be achieved with a bed of 80L or more. At higher bed volume, an increase of volume doesn't seem to increase the performance of the VPSA cycle, which is represented by a merge of the 80,100,120 and 140 L lines. At 1.1 bar, the targets of the CO₂ capture process are not met with a purity of maximum 77% for a recovery of 90%.

For the 2 bar plot, an increase of volume also increase the performance of the VPSA, as the 1.1 bar plot, but the effect of bed volume increase is more pronounced, and there does not seem to be a limit to this increase contrary to the case at 1.1 bar. In this case, the desired targets (at least 90% of recovery and 95% of purity) are barely met with a bed volume of 100 L. At 120 L and 140 L, several points are above these targets.

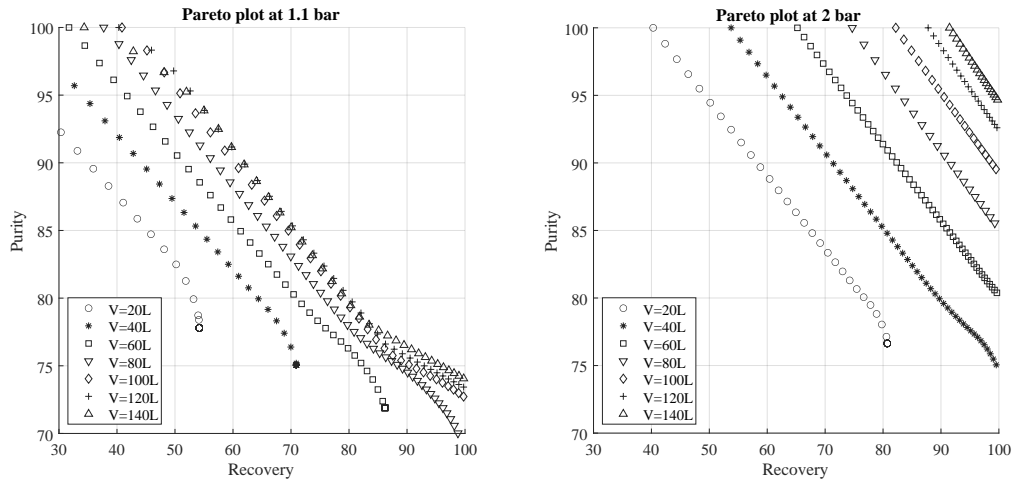


Fig. 9. Purity versus recovery obtained for different volumes of individual adsorption bed at two different adsorption pressure for the 3bed-6step cycle.

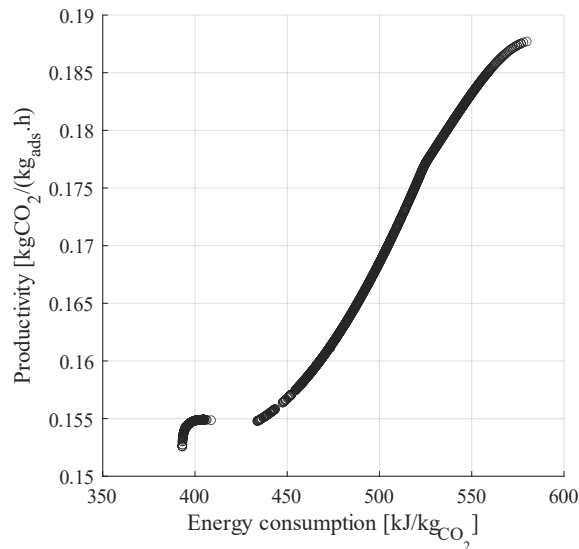


Fig. 10. Pareto plot of productivity versus energy consumption obtained for a recovery of at least 90% and purity of at least 95%.

Since the targets are reached with this cycle, an optimization of productivity and energy consumption was made in order to find the best operating conditions giving the desired purity and recovery. Nevertheless, there is a trade-off between productivity and energy consumption. A pareto plot was made by optimizing these two indicators for a purity of 95% or higher and a recovery of 90% or higher. This pareto plot is represented in Figure 10. As represented, the lowest energy consumption reachable is 393.1 $\text{kJ/kg}_{\text{CO}_2}$, giving a productivity of 0.1526 $\text{kgCO}_2/(\text{kg}_{\text{ads}}\cdot\text{h})$. Starting from the lowest energy consumption, we can observe two distinct areas. The first is located at the lowest energy consumption and productivity. We can observe a L-shape where the productivity starts to decrease quickly when the

lower bound of energy consumption is approached. In this area, the volume of the column is equal to 120 to 140 L, which gives the best energy consumption but low productivity. In the second area, the size of the bed begins to decrease, showing an increase of productivity but also an increase in energy consumption. The highest productivity obtained is $0.1877 \text{ kg}_{\text{CO}_2}/(\text{kg}_{\text{ads}}\cdot\text{h})$ with an energy consumption $579.8 \text{ kJ}/\text{kg}_{\text{CO}_2}$. There is no optimal value since the choice depends on the price of the MOF for the productivity, and the price of electricity for the energy consumption. The operating conditions of the 2 extrema are given in the Table 4. It is also interesting to note that the energy consumption and productivity are better than the two-column cycle for both cases.

Table 4. Operating conditions for three optima reaching the targets of purity and recovery for the 3bed-6step cycle

	Best energy consumption	Best productivity
Adsorption time [s]	200	139
Purge time [s]	168.2	119
Light blowdown time [s]	10	10
Adsorption pressure [bar]	2	2
Middle pressure [bar]	1.44	1.26
Blowdown pressure [bar]	0.1	0.1
Purge flow rate [Nm^3/h]	5	5
Volume of the bed [L]	127	100
L/D ratio [/]	2	3.5
Purity [%]	95.73	95
Recovery [%]	90	90
Productivity [$\text{kg}_{\text{CO}_2}/(\text{kg}_{\text{ads}}\cdot\text{h})$]	0.1526	0.1877
Energy consumption [$\text{kJ}/\text{kg}_{\text{CO}_2}$]	393.1	579.8

4. Conclusions

In this work, the performances of the shaped MIL-160(AI) were evaluated from a laboratory scale to an small industrial pilot scale (TRL-6). Adsorption isotherm measurements were performed and modelled, showing good working capacity and selectivity for CO_2 . A breakthrough curve measurement was performed to determine the kinetic parameters of the adsorption by fitting of the breakthrough curve. The results obtained from adsorption isotherms and breakthrough curve allow to simulate two VPSA cycles in Aspen Adsorption V11 software.

Recovery and purity optimum for the 2 bed-5step cycle were investigated at 1.1 and 2 bar for different volumes of adsorption columns. In this cycle, it seems to have an optimum bed size for the treated flow rate which is around 80L. Above this value the performance of the cycle starts to decrease at 1.1 bar and remain identic at 2 bar. The targets of a CO_2 capture process are not met with a single unit of 2 beds, and a second unit was investigated to reach the desired performance. The two units were optimized to reach a purity of 95% and a recovery of 90%. Nevertheless, the best results obtained give a recovery of 90% and a purity of 88%.

A second cycle was studied to reach the desired performances with a single unit. The 3bed-6step cycle was studied and optimized. The results shown that the objectives can be reached with an adsorption bed of at least 100 L and with an adsorption pressure of 2 bar. The cycle was then optimized to find the best productivity and energy consumption for the targets. In order to make a complete comparison with absorption-regeneration capture in amines, the energy consumption of pre-treatment should be taken into account in a simulation of the complete CO_2 capture chain. The results obtained from theses simulations are promising and will be compared to the Technology Centre Mongstad pilot plant which is a demonstration site of the MOF4AIR project.

References

- [1] IPCC. Summary for policymakers. Climate Change 2021: The Physical Science Basis. Contribution of Working Group I to the Sixth Assessment Report of the Intergovernmental Panel on Climate Change, 2021.
- [2] Joeri Rogelj, Michel Den Elzen, Niklas Höhne, Taryn Fransen, Hanna Fekete, Harald Winkler, Roberto Schaeffer, Fu Sha, Keywan Riahi, and Malte Meinshausen. Paris Agreement climate proposals need a boost to keep warming well below 2°C. *Nature*, 534(7609):631–639, 2016.
- [3] Pierre Fridlingstein, et al. Global Carbon Budget 2020. *Earth System Science Data*, 12(4):3269–3340, 2020.
- [4] UNFCCC. Greenhouse Gas Inventory Data - Detailed data by Party, 2019. https://di.unfccc.int/detailed_data_by_party.
- [5] Praveen Bains, Peter Psarras, and Jennifer Wilcox. CO₂ capture from the industry sector. *Progress in Energy and Combustion Science*, 63:146–172, 2017.
- [6] Samer Fawzy, Ahmed I. Osman, John Doran, and David W. Rooney. Strategies for mitigation of climate change: a review. *Environmental Chemistry Letters*, 18(6):2069–2094, 2020.
- [7] Najmus S. Sifat and Yousef Haseli. A critical review of CO₂ capture technologies and prospects for clean power generation. *Energies*, 12(21), 2019.
- [8] Mohammad Younas, Mashallah Rezakazemi, Muhammad Daud, Muhammad B. Wazir, Shakil Ahmad, Nehar Ullah, Inamuddin, and Seeram Ramakrishna. Recent progress and remaining challenges in post-combustion CO₂ capture using metal-organic frameworks (MOFs). *Progress in Energy and Combustion Science*, 80, 2020.
- [9] Efthymia Ioanna Koytsoumpa, Christian Bergins, and Emmanouil Kakaras. The CO₂ economy: Review of CO₂ capture and reuse technologies. *Journal of Supercritical Fluids*, 132(July 2017):3–16, 2018.
- [10] Kenji Sumida, David L Rogow, Jarad A Mason, Thomas M McDonald, Eric D Bloch, Zoey R Herm, Tae-hyun Bae, and R Long. Carbon Dioxide Capture in Metal-Organic Frameworks. *Chemical Rev*, 112:724–781, 2012.
- [11] F. Vega, F. M. Baena-Moreno, Luz M. Gallego Fernández, E. Portillo, B. Navarrete, and Zhien Zhang. Current status of CO₂ chemical absorption research applied to CCS: Towards full deployment at industrial scale. *Applied Energy*, 260(October 2019):114313, 2020.
- [12] NRG. Petra Nova - Carbon capture and the future of coal power, 2021. <https://www.nrg.com/case-studies/petra-nova.html>.
- [13] Debangsu Bhattacharyya and David C. Miller. Post-combustion CO₂ capture technologies a review of processes for solvent-based and sorbent-based CO₂ capture. *Current Opinion in Chemical Engineering*, 17:78–92, 2017.
- [14] Justin C. Glier and Edward S. Rubina. Assessment of solid sorbents as a competitive post-combustion CO₂ capture technology. *Energy Procedia*, 37:65–72, 2013.
- [15] Hsien H. Khoo and Reginald B.H. Tan. Life cycle investigation of CO₂ recovery and sequestration. *Environmental Science and Technology*, 40(12):4016–4024, 2006.
- [16] Luca Riboldi and Olav Bolland. Overview on Pressure Swing Adsorption (PSA) as CO₂ Capture Technology: State-of-the-Art, Limits and Potentials. *Energy Procedia*, 114(1876):2390–2400, 2017.
- [17] Carlos A. Grande. Advances in Pressure Swing Adsorption for Gas Separation. *ISRN Chemical Engineering*, 2012:1–13, 2012.
- [18] Daiane Damasceno Borges, Périne Normand, Anastasia Permiakova, Ravichandar Babarao, Nicolas Heymans, Douglas S. Galvao, Christian Serre, Guy De Weireld, and Guillaume Maurin. Gas Adsorption and Separation by the Al-Based Metal-Organic Framework MIL-160. *Journal of Physical Chemistry C*, 121(48):26822–26832, 2017.
- [19] Mohammad Wahiduzzaman, Dirk Lenzen, Guillaume Maurin, Norbert Stock, and Michael T. Wharmby. Rietveld Refinement of MIL-160 and Its Structural Flexibility Upon H₂O and N₂ Adsorption. *European Journal of Inorganic Chemistry*, 2018(32):3626–3632, 2018.
- [20] C W Skarstrom. Method and apparatus for fractionating gaseous mixtures by adsorption, 1960. U.S. patent 2, 944, 627.
- [21] Liu, Z., Grande, C. A., Li, P., Yu, J., & Rodrigues, A. E. Multi-bed vacuum pressure swing adsorption for carbon dioxide capture from flue gas. *Separation and Purification Technology*, 81(3), 307–317, 2011.
- [22] José A. Delgado, María A. Uguina, José L. Sotelo, Vicente I. Águeda, Abel Sanz, and Pilar Gómez. Numerical analysis of CO₂ concentration and recovery from flue gas by a novel vacuum swing adsorption cycle. *Computers and Chemical Engineering*, 35(6):1010–1019, 2011.
- [23] M. Khurana, S. Farooq. Simulation and optimization of a 6-step dual-reflux VSA cycle for post-combustion CO₂ capture. *Chem. Eng. Sci.*, 152 (2016), pp. 507–515
- [24] Krishnamurthy, S., Lind, A., Bouzga, A., Pierchala, J., & Blom, R. Post combustion carbon capture with supported amine sorbents: From adsorbent characterization to process simulation and optimization. *Chemical Engineering Journal*, 406, 127121, 2021
- [25] Philipp Brandt, Alexander Nuhnen, Marcus Lange, Jens Möllmer, Oliver Weingart, and Christoph Janiak. Metal-Organic Frameworks with Potential Application for SO₂ Separation and Flue Gas Desulfurization. *ACS Applied Materials and Interfaces*, 11(19):17350–17358, 2019.
- [26] Pengbo Lyu and Guillaume Maurin. H₂S Stability of Metal-Organic Frameworks: A Computational Assessment. *ACS Applied Materials and Interfaces*, 13(3):4813–4822, 2021.
- [27] Permyakova, Anastasia Aleksandrovna, Oleksandr Skrylnyk, Emilie Courbon, Maame Affram, Sujing Wang, U.-Hwang Lee, Anil H. Valekar, Farid Nouar, Georges Mouchaham, Thomas Devic, Guy De Weireld, Jong - San Chang, Nathalie Steunou, Marc Frere and Christian Serre. “Synthesis Optimization, Shaping, and Heat Reallocation Evaluation of the Hydrophilic Metal-Organic Framework MIL-160(Al).” *ChemSusChem* 10 7, pp. 1419–1426, 2017.
- [28] G. De Weireld, M. Frère, and R. Jadot. Automated determination of high-temperature and high-pressure gas adsorption isotherms using a magnetic suspension balance. *Measurement Science and Technology*, 10(2):117–126, February 1999.
- [29] A L Myers and J M Prausnitz. Thermodynamics of Mixed-Gas Adsorption. *A.I.Ch.E. Journal*, 11(1):121–127, 1965.
- [30] Pierre Billemont, Nicolas Heymans, Périne Normand, and Guy De Weireld. IAST predictions vs co-adsorption measurements for CO₂ capture and separation on MIL-100 (Fe). *Adsorption*, 23(2-3):225–237, 2017.

- [31] Amir H. Farmahini, Shreenath Krishnamurthy, Daniel Friedrich, Stefano Brandani, and Lev Sarkisov. Performance-Based Screening of Porous Materials for Carbon Capture. *Chemical Reviews*, 121(17):10666–10741, 2021.
- [32] Luca Riboldi and Olav Bolland. Overview on Pressure Swing Adsorption (PSA) as CO₂ Capture Technology: State-of-the-Art, Limits and Potentials. *Energy Procedia*, 114(1876):2390–2400, 2017.
- [33] Lu Wang, Zhen Liu, Ping Li, Jin Wang, and Jianguo Yu. CO₂ capture from flue gas by two successive VPSA units using 13XAPG. *Adsorption*, 18(5-6):445–459, 2012.
- [34] Irving Langmuir. The Adsorption of Gases on Plane Surfaces of Glass, Mica and Platinum. *Journal of the American Chemical Society*, 40(9):1361–1403, 1918.
- [35] Tolazzi, N., Steffani, E., Barbosa-Coutinho, E., Júnior, J. B. S., Pinto, J. C., & Schwaab, M. Adsorption equilibrium models: computation of confidence regions of parameter estimates. *Chemical Engineering Research and Design*, 138, 144-157, 2018
- [36] Douglas Ruthven. *Principles of Adsorption and Adsorption Processes*. John Wiley Sons, New York, first edition, 1984.
- [37] John Prausnitz, Rüdiger Lichtenthaler, and Edmundo Gomes de Azevedo. *Molecular Thermodynamics of Fluid-Phase Equilibria*. Prentice Hall PTR, New Jersey, third edit edition, 1999.
- [38] R Byron Bird, Warren E. Stewart, and Edwin N. Lightfoot. *Transport Phenoma*. John Wiley Sons, New York, second edi edition, 2002.
- [39] S. Sircar and J. R. Hufton. Why does the linear driving force model for adsorption kinetics work? *Adsorption*, 6(2):137–147, 2000.
- [40] T.H. Chilton, A.P. Colburn Mass transfer (absorption) coefficients prediction from data on heat transfer and fluid friction *Ind. Eng. Chem.*, 26 (1934), pp. 1183-1187
- [41] Frank P Incropera and David P DeWitt. *Fundamentals of Heat and Mass Transfer*, 1996.
- [42] Frank Kreith, Raj M.Manglik, and Mark S. Bohn. *Principles of Heat Transfer*. Cengage Learning, seventh edition, 2001.
- [43] Anthony G.Dixon.Wall and particle-shape effects on heat transfer in packed beds. *Chemical Engineering Communications*, 71(1):217–237, 1988.
- [44] Montgomery, Douglas C., George C. Runger, and Norma F. Hubele. *Engineering statistics*. John Wiley & Sons, 2009.